

VLBI Observations of NGC6240: resolving the double nuclei and radio supernovae

Yoshiaki Hagiwara¹

National Astronomical Observatory of Japan, 2-21-1, Osawa, Mitaka, 181-8588 Tokyo, Japan
yoshiaki.hagiwara@nao.ac.jp

Willem A. Baan²

ASTRON, PO Box 2, 7990 AA Dwingeloo, The Netherlands
and

Hans-Rainer Klöckner³

University of Oxford, Denys Wilkinson Building, Keble Road, Oxford OX1 3RH, United Kingdom

ABSTRACT

The European VLBI Network (EVN) has been used at two epochs in 2003 and 2009 to obtain multi-frequency high-resolution images of the merger galaxy NGC 6240 in order to study the radio properties of all compact high-brightness components in the galaxy. Our observations at milli-arcsecond resolution detected the northern and southern nuclei and two radio components, which we interpret as long-lived luminous supernovae associated with the circum-nuclear starburst activity at the southern nucleus. The new VLBI data support the presence of an active galactic nucleus (AGN) together with starburst activity at the southern nucleus and provides some evidence for an AGN at the northern nucleus. The two nuclei both display an inverted spectrum at lower GHz frequencies. The spectrum of the southern nucleus indicates thermal free-free absorption on parsec scales, consistent with the presence of an AGN.

Subject headings: galaxies: active — galaxies: individual (NGC 6240) — galaxies: starburst — radio continuum: galaxies — supernovae: general

1. Introduction

The merging galaxy NGC 6240 has a large far-infrared (FIR) luminosity of $L_{\text{FIR}} = 3.5 \times 10^{11} L_{\odot}$ (Yun & Carilli 2002) and belongs to the category of luminous infrared galaxies (LIRGs; $L_{\text{IR}} = 10^{11} - 10^{12} L_{\odot}$) (see Sanders & Mirabel 1996, for a review). The large luminosity of these LIRGs

and Ultra-Luminous Infrared Galaxies (ULIRGs; $L_{\text{IR}} = 10^{12} - 10^{13} L_{\odot}$) is likely to be dominated by starburst activity induced by galaxy-galaxy interactions, where the UV radiation from massive star formation is reprocessed to far-infrared radiation in the dusty environment (e.g., Sanders et al. 1988; Sanders & Mirabel 1996; Skinner et al. 1997). The NGC 6240 merging system has been described at optical wavelengths (Fried & Schulz 1983) and is thought to host an active galactic nucleus (AGN) in its nuclear region (e.g., Depoy, Becklin, & Wynn-Williams 1986). The two galactic nuclei found in the central region have a projected separation between $1''.5$

¹Department of Astronomical Science, The Graduate University for Advanced Studies (Sokendai), 2-21-1, Osawa Mitaka, 181-0015 Tokyo, Japan

²Department of Mathematics, Physics and Computer Science, Linnaeus University, 351 95 Växjö, Sweden

³Max-Planck-Institut für Radioastronomie, Auf dem Hügel 69, 53121 Bonn, Germany

and $1''.8$ ($0.714\text{--}0.856$ kpc) at X-ray and radio wavelengths (Fried & Schulz 1983; Beswick et al. 2001; Komossa et al. 2003; Gallimore & Beswick 2004; Max et al. 2007). Because the northern nucleus, with the highest absorbing column densities, lies well behind the southern nucleus (Baan, Hagiwara & Hofner 2007), the separation varies as the intervening hot (obscuring) dust becomes optically thinner at longer wavelengths (Max et al. 2007). X-ray observations at 2–10 keV reveal the presence of iron line emission at 6.4 keV at both nuclei, which is most prominent in the southern nucleus and classifies this as a binary AGN (Komossa et al. 2003).

Thermal CO emission reveals a significant mass concentration that is centered between the two nuclei (Tacconi et al. 1999; Bryant & Scoville 1999; Nakanishi et al. 2005; Iono et al. 2007) and largely consists of interstellar gas (Scoville et al. 2000). This intervening molecular gas concentration results from a superposition of disk gas from the two merging galaxies, which is confirmed by the structure and peak location of the OH absorption structure against the extended radio emission of the nuclear region (Baan, Hagiwara & Hofner 2007).

Radio observations at centimeter wavelengths of the central $2''$ region of NGC 6240 using the NRAO Very Large Array display the two nuclei and an extended northern structure (N3) that is part of the large-scale loop structure to the west of the nuclear source (Colbert et al. 1994; Baan, Hagiwara & Hofner 2007). A large scale diffuse component envelops these three structural components. The nuclear radio components remain unresolved at higher resolution at 5 GHz using MERLIN (Beswick et al. 2001). The loop structures including N3 have been resolved away at this resolution and the southern nucleus, N1 shows east-west structure at its lowest contours ($PA = 60^\circ$) and a northern extension ($PA = -30^\circ$).

At milli-arcsecond resolution using the NRAO Very Long Baseline Array (VLBA), the northern nucleus N2 also displays a multi-component east-west structure suggesting a core with a two-sided jet (Gallimore & Beswick 2004). The southern nucleus has a peak central structure surrounded by weak additional components possibly related to starformation. Both high-brightness nuclei show an inverted spectrum at lower frequency with a spectral turn-over or flatness due to free-

free absorption (FFA) or possibly synchrotron-self absorption (SSA) (Gallimore & Beswick 2004). Strong H_2O maser emission was discovered (e.g., Hagiwara et al. 2002) at the exact center of the southern nucleus (Hagiwara et al. 2003; Hagiwara 2010), which may be related to a dense molecular gas around a central engine.

Here, we present European VLBI Network (EVN) observations with increased surface brightness sensitivity to image the compact sources at increasing frequencies. New EVN observations at 1.6, 2.2, 5.0 and 8.4 GHz were made to study the source structure, the overall spectral energy distribution, and to check for consistency with the earlier VLBA results. In Section 2 we present the new observations, the data analysis, and the observational results, including the identification and morphology of all detected compact radio sources. In Section 3 we discuss the nature of these sources and compare NGC 6240 with other active galaxies. Finally, in Section 4 we summarize the discussion.

Cosmological parameters of $H_0 = 73$ km $s^{-1}Mpc^{-1}$, $\Omega_\Lambda = 0.73$, and $\Omega_M = 0.27$ are adopted throughout this article, which results in a luminosity distance of NGC 6240 of 103 Mpc at $z = 0.0245$ and an angular conversion of 1 arcsec equaling 476 pc in linear scale. The designation of radio components follows that defined in Colbert et al. (1994) with N1 being the southwestern nucleus and N2 being the northeastern nuclei. The two nuclei were called respectively S and N1 in Gallimore & Beswick (2004).

2. Imaging the double nuclei in NGC 6240

2.1. Observations and imaging

The European Very Long Baseline Interferometry Network (EVN) has been used to observe the nuclear region of NGC 6240 in order to investigate the nature of the active galactic nuclei and nuclear starbursts in the galaxy. The stations used for these observations at two epochs in 2003 and 2009 were Effelsberg (Ef), Hartebeesthoek (Hh), the 76-m Lovell telescope (Jb) at Jodrell Bank, Medicina (Mc), Noto (Nt), Onsala (On), Shanghai (Sh), Torun (Tr), Urumqi (Ur), and the Westerbork (Wb) phased-array. A summary of the observational details is presented in Table 1. All observations were conducted in phase-referencing mode at all frequency bands using the nearest calibration

source J1651+0129 (centered at R.A.(J2000) = $16^{\text{h}}51^{\text{m}}03^{\text{s}}.6620$, Dec.(J2000) = $01^{\circ}29'23''.458$) at 1.01° away from NGC 6240. Only the Lovell telescope did not participate in the phase-referencing part of the observations due to its lower slewing rate.

The first epoch observations at 1.6 GHz and 5.0 GHz were made on 30 October and 10 November, 2003 and utilized a 32 MHz total bandwidth with 2 bit sampling in dual-circular polarization mode for a total data recording rate of 256 Mbit s^{-1} . Observations of 2.5–3 minutes on the target were interleaved with observations of 1.5–2 minutes on the phase-referencing source, which gave about 4.2 hours total on-source time.

Second epoch observations at 5.0 GHz, 2.2 GHz, and 8.4 GHz were made on 16, 17 June, 2009. The observations at 5.0 GHz were made in dual-circular polarization mode utilizing 64 MHz total bandwidth with 2 bit sampling for a total data recording rate of 512 Mbit s^{-1} . Three minute scans on the target were alternated with one minute scans on the phase-referencing source, which resulted in 5.7 hours total on-source time. The observations at 2.2 and 8.4 GHz were made in single polarization mode with the S/X dual-frequency receiving system with a bandwidth of 128 MHz at each frequency and 2 bit sampling for a total recording rate of 512 Mbit s^{-1} . Three minute scans on the target and one minute scans on the phase-referencing source were alternated during the observation, which resulted in 2.9 hrs total on-source time at each frequency. All observations were done with the same reference position near the southern nucleus of NGC 6240 (R.A.(J2000) = $16^{\text{h}}52^{\text{m}}58^{\text{s}}.8903$, Dec.(J2000) = $02^{\circ}24'03''.339$).

The data were correlated using the EVN MkIV correlator at the Joint Institute for VLBI in Europe (JIVE) and the output visibility data were averaged to 1-2 seconds. Sixteen frequency channels of 500 kHz were used across each 8 MHz band. Data calibration and imaging were carried out in the NRAO Astronomical Image Processing System (AIPS). After initial data editing, the delay error corrections resulting from ionospheric effects were applied to all visibility data. A-priori amplitude calibration was performed using the system temperature and gain information provided for each telescope. The delays and fringe rates

for the calibration sources 3C 273 or 3C 345, and J1651+0129 were applied to the target source, NGC 6240. Using the measured flux densities of the phase-referencing source J1651+0129 at 2 epochs as a basis, the relative accuracy of the target flux densities is estimated to be $\sim 10\%$. This error estimate includes the effects of bandwidth and time smearing and ionospheric delays, which are estimated to be several percent for these EVN observations.

Cleaned images of 512×512 pixels were produced, one centered near the southern nucleus and one at the intensity peak position of the northern nucleus offset by $0''.5051$ in right ascension and $1''.4279$ in declination from the phase center. The noise levels of 1–2 times theoretical noise and synthesized beams from CLEAN-ed images are summarized in Table 2. Self-calibration could not be applied successfully because of the low signal-to-noise ratio of the images. Final images have been phase-referenced to the nearby calibrator J1651+0129. Because of residual errors in the calibration of the phase-reference sources, the associated structure at the lowest contours ($\lesssim 3 \sigma$ or 4σ) in the source images may not be reliable.

The positions of the radio components and their errors at the peak brightness at each frequency and both epochs are listed in Table 3. These composite position errors have been estimated from the theoretical thermal noise errors of interferometer phase (e.g., Thompson et al. 1986), the systematic errors of the phase-referencing VLBI observations (σ_{phr}), and the errors of the absolute position of the phase-referencing source (σ_{ref}), using the quadrature equation: $\sqrt{(\theta/2SNR)^2 + \sigma_{\text{phr}}^2 + \sigma_{\text{ref}}^2}$. Here θ represents the synthesized beam size and SNR represents the signal-to-noise ratio. The values of σ_{phr} ($\Delta\alpha \cos\delta = 0.060 \text{ mas}$, $\Delta\delta = 0.020 \text{ mas}$) are obtained from the simulated astrometric accuracy of the EVN array (Pradel et al. 2006), adopting a separation between calibrator and target of 1.0° at position angle 152.2° and at an approximate source declination of 0° . The value of σ_{ref} is 0.58 (mas) from the VLBA Calibrator List (Kovalev et al. 2007). Table 4 lists the flux densities of the radio components at each observing frequency, which also includes two weaker components appearing in the earlier VLBA observations (see Figures 2, 3, and 4 in Gallimore & Beswick

2004). Source sizes of these components in Table 5 are measured from the final images using the AIPS task JMFIT. Assuming Gaussian distributions for sources, the upper limits of the source sizes have estimated accuracies of 3–30% depending on observing frequency and epoch. Table 6 presents the properties of the radio sources detected in our observations.

2.2. Source identification and morphology

The new VLBI maps obtained from 1.6–8.4 GHz display four compact high-brightness emission components as identified in Figure 1: the nuclei, N1(south) and N2(north) identified in earlier interferometric observations (Beswick et al. 2001; Hagiwara et al. 2003) and two new components RS1 and RS2 near the southern nucleus. The radio source RS1 was first identified southwest of the southern nucleus at 5.0 GHz in October, 2003 and it is detected at 5.0 and 8.4 GHz in June, 2009 (see Figure 2). The other radio source RS2 was identified northeast of the southern nucleus at Epoch 1 and was more prominent at 1.6 GHz than at 5.0 GHz (see Figure 4). At Epoch 2 the source RS2 was clearly detected at 5.0 GHz but not at 2.2 GHz with an upper limit flux density of $2.75 \text{ mJy beam}^{-1}$. All diffuse emission in the central $2''$ region, observed in earlier Very Large Array observations (e.g. Colbert et al. 1994; Baan, Hagiwara & Hofner 2007), has been resolved out.

The VLBA observation at 8.4 GHz of August 1999 did not detect the two nuclei at a 5σ upper limit of $0.65 \text{ mJy beam}^{-1}$ (Gallimore & Beswick 2004), but the northern nucleus was detected at 8.4 GHz in June 2009 with similar sensitivity, which suggests some intensity variability of the northern nucleus. Both nuclei were detected at 5 GHz at both Epochs. Their peak positions in the EVN data (Table 3) agree at all frequencies with earlier VLBA measurements using estimated uncertainties of 0.6 mas in right ascension and 1.5 mas in declination (Gallimore & Beswick 2004). The 5.0 GHz maps in Figures 2 and 3 display the two nuclear components N1 and N2 obtained at Epoch 1 and Epoch 2, respectively. The southeastern nucleus, N1 was not detected at the highest frequency of 8.4 GHz with an upper limit of $0.55 \text{ mJy beam}^{-1}$ (Figure 2). Individual source maps indicate that the sources N1 and N2 are resolved

but that the minor axis of RS2 northeast of N1 is unresolved (Figure 4). The peak of RS1 is separated from N1 by 23.3 mas at 5.0 GHz at a position angle of $\sim 35^\circ$, corresponding to 11.1 pc at the distance to NGC 6240. At the lowest frequency of 1.6 GHz, N1 and RS1 are not spatially separated. Also, RS1 was not detected at 2.2 GHz at Epoch 2 possibly because of the lower signal-to-noise ratio.

The source RS2 is located northeast of the southern nucleus in our 1.6 GHz EVN map of Figure 4. It appears that the peak position of RS2 at 1.6 and 5.0 GHz lies close to the compact component S1 at $0''.3$ northeast from N1 in the 1.7 and 2.4 GHz VLBA observations (Gallimore & Beswick 2004). On the other hand, RS2 has an offset of $\approx 10\text{--}15$ mas at 1.6 GHz or 5.0 GHz relative to S1 at 1.7 GHz or 2.4 GHz, which is not within the estimated positional errors (Table 3). Therefore, RS2 is a different source to S1 in the earlier VLBA data. We interpret both components to be part of the circum-nuclear star-forming region that extends over 10 mas or ~ 5 pc around N1.

The structure of the northeastern nucleus N2 at 5.0 GHz (Figure 3) shows a northwest extension of $\approx 0''.02$ (≈ 9.5 pc) that is consistent with the earlier VLBA maps at 1.7 and 2.4 GHz (Gallimore & Beswick 2004). Although this structure at lower contours may not be reliable because of incomplete phase and amplitude calibration, an east-west structure may be explained as a core-jet structure typically seen in high-luminosity Seyfert nuclei. The northern nucleus itself remains unresolved at both 1.6 and 2.2 GHz. Only at the highest frequency of 8.4 GHz, N2 has an east-west elongation that is consistent with the earlier VLBA data (Figure 3).

3. Discussion

Our EVN data present the detection of the double nuclei at higher frequencies of 5.0 and 8.4 GHz, where earlier VLBA data failed to detect these nuclei. These results combined with earlier VLBA studies, allow study of the nature of the nuclei at milliarcsecond-scale structure. While our study focuses on the physics of the two nuclei, the detection of two new components is a key to understanding the activity of NGC 6240.

3.1. The northern nucleus N2

The northern nucleus N2 shows an inverted spectrum rather than a steep spectrum that would be more typical for a radio jet (Figure 5). The structure of N2 at 5.0 GHz is partially resolved and shows an east-west extension at its lower contours that still remains questionable because of the insufficient amplitude calibration (Figure 3). Changes in source structure may also result from a different (u,v) coverage for the two epochs. The detection of the X-ray emission towards N2 (Komossa et al. 2003) is less convincing than the definite detection towards N1. Nevertheless, the radio morphology of N2 resembles that of a core-jet structure seen in Seyfert nuclei, such as NGC 1068 (Gallimore et al. 2004), but this requires further verification. By contrast with Arp 299, the VLA observations of the H₂O maser in NGC 6240 have not detected any emission towards N2 during seven years (Hagiwara et al. 2003; Hagiwara 2010).

3.2. The southern nucleus N1

The southern nucleus N1 appears partially resolved in an east-west direction (Figure 2b,2c) but its flux density at 5.0 GHz has not changed significantly during 6 years. Contrary to the spectrum of N2 (see discussion below), the spectrum of N1 with missing Epoch 2 detections at 2.2 and 8.4 GHz may not be inverted (Figure 5), although its spectral shape (including upper limits) strongly indicates a spectral turnover around 2.0 GHz. The non-detection of N1 at 8.4 GHz suggests a relatively flat AGN-like spectrum and a lower limit for the spectral index $\alpha < 0.55$ between 5.0 and 8.4 GHz, using $S_\nu \propto \nu^\alpha$ with S_ν being the flux density at frequency ν . In addition, the radio brightness temperature $> 10^6$ K (Table 6) and the detection of strong hard X-ray emission and neutral iron line emission would argue for the presence of an AGN in N1. Considering the available evidence, the southern nucleus may host both an AGN and a (circum-)nuclear starburst region.

The H₂O maser features in NGC 6240 nearly coincide with the continuum peak of the southern nucleus (Hagiwara et al. 2003; Hagiwara 2010). The narrow H₂O maser lines are redshifted by $\sim 200\text{--}300$ km s⁻¹ with respect to the systemic velocity of N1 (e.g., Hagiwara 2010;

Baan, Hagiwara & Hofner 2007) and may originate in the receding side of a compact rotating molecular disk at the nucleus (e.g., Miyoshi et al. 1995), which would also support the presence of an AGN. Alternatively, these narrow lines distributed over 120 km s⁻¹ could be explained by wind maser emission as observed in the Circinus galaxy (Greenhill et al. 2003).

The southern nucleus N1 of NGC 6240 has characteristics that are comparable with those of component A of Arp 299 (Neff et al. 2004; Ulvestad 2009). The 8.4 GHz radio power of N1 of ($P_{N1} = 3.7 \times 10^{22}$ W Hz⁻¹) (Colbert et al. 1994) is only a factor of two more than the 8.4 GHz power of nucleus A of Arp 299 ($P_A = 1.8 \times 10^{22}$ W Hz⁻¹ and $P_{B1} = 2.9 \times 10^{21}$ W Hz⁻¹) (Neff et al. 2004). The compact source A of Arp 299 has been resolved into discrete sources at milliarcsecond-scale by recent EVN observations and one of these sources (A1) is the AGN candidate with a flat spectral index of -0.13 ± 0.11 (Pérez-Torres et al. 2010). Five bright and compact radio sources lie within 10 pc and are candidates of Type-II young radio supernovae (Neff et al. 2004). Four of these five radio sources have flat or inverted radio spectra between 2.2 and 8.4 GHz, very similar to RS1 and RS2 near N1 in NGC 6240. The luminous H₂O maser emission in Arp 299 is found towards both nuclei A and B1 (Henkel et al. 2005) and at A it coincides with its continuum peak at VLA resolution (Tarchi et al. 2010). While this spatial coincidence may also suggest an AGN association (e.g., Hagiwara 2007), the maser in Arp 299 is blueshifted relative to the systemic velocity and is likely associated with an outflow in a starforming environment.

3.3. Spectral analysis of N1 and N2

In order to understand the observed spectra of the southern and northern nuclei, model fitting may be used to explain the frequency turnover at lower frequencies using a power-law plus pure free-free absorption (FFA) or synchrotron self-absorption (SSA) (e.g., Kamenov et al. 2000). First, the FFA model for a nuclear spectrum is described by:

$$S_\nu = S_0(\nu/1.0)^{\alpha_0} \exp\{-\tau_{\text{ff}}(\nu/1.0)^{-2.1}\}, \quad (1)$$

where ν is the frequency in GHz, S_0 is the unobscured synchrotron flux density in mJy, α_0 is the

optically thin non-thermal spectral index, and τ_{ff} is the opacity at 1.0 GHz. This model describes all FFA in the foreground to the synchrotron emission source and assumes that all source components are subject to the same foreground opacity (e.g., Parra et al. 2007). The second model of pure SSA is described as follows:

$$S_\nu = S_0 \nu^{2.5} [1 - \exp\{-\tau_s \nu^{\alpha_0 - 2.5}\}], \quad (2)$$

where ν is the frequency in GHz, $S_0 \tau_s$ will be close to the flux density, if the SSA coefficient $\tau_s \ll 1$, and α_0 is the optically thin non-thermal spectral index.

The parameters of the FFA and SSA spectral fits for N1 and N2 and the reduced χ^2 values (per degree of freedom) have been summarized in Table 7, and the fitted curves are shown in Figure 5. Both the FFA and SSA models produce reliable fits for N1 with low values (< 1.5) for the reduced χ^2 with the FFA model being slightly worse but does not make good fits to N2. However, since there is no compact source in N1 or N2 having a high brightness temperature, any synchrotron self-absorption in these nuclei is unlikely (Kellermann & Pauliny-Toth 1969). Using conventional energy equipartition arguments at lower radio frequencies, a turn-over frequency of 2.0 – 3.0 GHz for a self-absorbed source requires an equipartition brightness temperature of $\sim 10^{11.95}$ K (Readhead 1994). The observed brightness temperatures for our sources are only $\sim 10^6 - 10^7$ K. Better constraints of the nuclear properties of N1 in terms of model fitting requires more complete flux density measurements.

While for N2 neither the pure FFA nor the pure SSA model can perfectly explain the spectral bending at 2–3 GHz (see Table 7 and Figure 5), the observed bending does indicate that free-free self-absorption by ionized foreground gas in a starburst environment is relevant. Since there is also no hint of self-absorption in the MERLIN spectrum (Beswick et al. 2001), the size of such an absorbing medium must be very small and between about 9.5 and 25 pc in linear size (Gallimore & Beswick 2004). Similarly, the presence of an AGN in N2 cannot be confirmed from our EVN data, except that the core-jet like structure, as also seen in the 1.7 and 2.4 GHz VLBA images, could support the presence of an active nucleus.

3.4. Radio sources near the southern nucleus RS1, RS2

The radio source RS1 has a radio power at 8.4 GHz of $4.1 \times 10^{21} \text{ W Hz}^{-1}$ and a spectral index of $\alpha_{5.0-8.4} \approx 0.34$ in our Epoch 2 observations. The radio power of RS2 at 5.0 GHz ($\alpha_{1.6-5.0} \approx -0.91$) is $7.5 \times 10^{20} \text{ W Hz}^{-1}$. The radio power of RS2 is comparable with those of the VLBI sources associated with the nucleus A in Arp 299 while the power of RS1 is nearly a factor ten higher, which makes it 1250 times the 8.4 GHz radio power of Cas A of $6 \times 10^{17} \text{ W Hz}^{-1}$ (Colbert et al. 1994). Both RS1 and RS2 display a radio light curve with a long-term rise (Figure 6). The upper limit for the source size of RS1 at the highest frequency 8.4 GHz is $1.5 \times 0.6 \text{ pc}$ (Table 5) and the source is not sufficiently resolved by our EVN synthesized beam. Also, different EVN beams resulting from different (u,v) coverage at each epoch make it difficult to make a reliable comparison of the intrinsic source sizes.

Speculation that RS1 could be the true southern nucleus, instead of N1, may be ruled out because RS1 was not detected in the 8.4 GHz VLBA observations (1999–2001) and only appeared in 2003. Also its location is significantly offset from the positions of N1 in the 2.4 and 1.7 GHz VLBA data. Similarly, the possibility that RS1 represents ejecta from the active nucleus N1 may be ruled out because its offset (11 pc) from N1 remained unchanged during 6 years and because RS1 is far from the known outflow structures seen in HI and OH southwest of N1 (Baan, Hagiwara & Hofner 2007). The positional difference of 10 mas ($\approx 50 \text{ pc}$) (see Table 3) between RS2 at 1.6 and 5.0 GHz and the source S1 at 1.7 and 2.3 GHz in VLBA observations at epochs in 2000 and 2001 suggests that they are also different sources.

The radio sources RS1 and RS2 have remained detectable for more than 6 years since 2003. An important question is whether these sources are supernovae (SNe, interacting with the circumstellar matter) or supernova remnants (SNRs, interacting with the dense ISM). There is no evidence for expanding supernovae shells with the highest beam size of $\sim 6 \text{ mas}$ ($\sim 3 \text{ pc}$) both in RS1 and RS2 between the two epochs from our data (see Table 5). The range of radio luminosity of $10^{20.8-21.6}$

W Hz⁻¹ of RS1 and RS2 is similar to the radio luminosity obtained for observed Type Ib/c or Type II radio supernovae (RSNe) (Weiler et al. 2002). Thus, it is possible that RS1 and RS2 are SNe or SN-SNR transition objects. Our data is insufficient to distinguish between the two cases and further sensitive VLBI monitoring would be required. The VLBA data (1999–2001) also displays two similar but weaker RSN or SNR candidates RS3 and RS4, the latter of which has a spectral index of $\alpha_{1.7-2.4} \approx 0.35$.

Many nearby galaxies, such as the LIRG M 82, and ULIRGs Arp 220 and Arp 299, display compact radio sources that are evidence of ongoing (circum-)nuclear starformation (Smith et al. 1998; McDonald et al. 2001; Neff et al. 2004; Parra et al. 2007; Conway et al. 2007; Ulvestad 2009). VLBI observations of the merging galaxy Arp 220 have detected a total of 18 compact radio sources within the western nucleus of the galaxy, over half of which have radio properties that are consistent with Type-II supernovae interacting with the surrounding medium (Parra et al. 2007). Likewise, the nuclei in Arp 299 show 30 compact radio sources, 25 of which are associated with the northeastern nucleus A (with an AGN candidate) and are spread over a region of 30 pc (Neff et al. 2004; Ulvestad 2009).

A comparison of the SN–SNR sources in NGC 6240 with those found in other sources shows that the radio powers of RS1 and RS2 are equivalent to those of the most powerful sources found in M 82 (see Fenech et al. 2008), although they are less powerful than those in Arp 220. As a result the upper limits for the sizes of RS1 and RS2 lie in the upper range of the general relation between radio luminosity and diameter observed for Galactic and extragalactic SNR sources (Berezhko and Völk 2004; Batejat et al. 2010). This would suggest that the environmental conditions in the LIRG NGC 6240, and possibly the star formation initial mass function, cannot yet be distinguished from those of the most luminous FIR galaxies.

4. Summary

We have conducted multi-frequency EVN observations of the nuclear region of the merging galaxy NGC 6240 at two epochs. The new VLBI maps reveal the double radio nuclei of NGC 6240

at milliarcsecond resolution, that are consistent with the earlier VLBI images obtained with the VLBA (Gallimore & Beswick 2004). The radio spectra from both nuclei suggest a spectral turn-over between 2 and 3 GHz. The spectrum of the southern nucleus N1 may be explained in terms of free-free absorption, although this explanation is still limited by having source flux densities with insufficient frequency coverage at each epoch. There is no clear interpretation for the spectrum of the northern nucleus N2.

Questions still remain about the true nature of the two radio nuclei and whether they both contain a radio-quiet AGN, a simple starburst, or a composite with an AGN and a circum-nuclear starburst. We suggest that the southern nucleus hosts an AGN and a circum-nuclear starburst, as evidenced by the X-ray data and the radio sources. The association of the H₂O maser with the nuclear source is still unknown. However, it is not clear that our data, together with earlier VLBA measurements, confirm the presence of an AGN at the northern nucleus.

The radio components RS1 and RS2 could be interpreted as long-lived radio supernovae that result from ongoing circum-nuclear star formation at N1. The radio spectrum of both sources is relatively flat and their location remains unchanged within error over about 6 years. More radio supernovae may have been detected in earlier observations around the active nucleus of N1, which groups NGC 6240 together with other well-known starburst nuclei that display RSNe or SNRs in their nuclei, such as M 81, M82, Arp 220 and Arp 299 (Bartel 2009). Radio interferometric observations are a powerful method to identify ongoing nuclear starformation and detect radio supernovae and supernova remnants in extragalactic sources.

We are grateful to Drs. Yoshiharu Asaki and Seiji Kamenno for their helpful suggestions, and we also thank to Dr. Robert Beswick for providing the MERLIN radio image. The authors thank Dr. Bob Campbell and other staff members in JIVE for their assistance in the observations, correlation, and data analysis. The authors also wish to thank an anonymous referee for suggestions that improved the manuscript. YH acknowledges Dr. Phil Edwards and staff members in VLBI Space Observatory Programme 2 (VSOP-

2) for providing valuable advice. The European VLBI Network is a joint facility of European, Chinese, South African and other radio astronomy institutes funded by their national research councils. This work was supported in part by The Graduate University for Advanced Studies (Sokendai). This research has made use of NASA's Astrophysics Data System Abstract Service. This research has made use of the NASA/IPAC Extragalactic Database (NED), which is operated by the Jet Propulsion Laboratory, California Institute of Technology, under contract with the National Aeronautics and Space Administration.

REFERENCES

- Baan, W. A., Hagiwara, Y., & Hofner, P. 2007, *ApJ*, 661, 173
- Ballo, L., et al. 2004, *ApJ*, 600, 634
- Bartel, N. 2009, in *Approaching Micro-Arcsecond Resolution with VSOP-2: Astrophysics and Technologies*, ed. Hagiwara, Y., Fomalont, E., Tsuboi, M., & Yasuhiro, M. (ASP Conf. Ser. 402) (San Francisco, CA: ASP), 243
- Batejat, F., Conway, J. E., Diamond, P. J., Parra, R., Lonsdale, C. J., Lonsdale, C. J. 2010, *astro-ph:arXiv:1011.4063v1*
- Berezhko, E. G., & Völk, H. J. 2004, *A&A*, 427, 525
- Beswick, R. J., Pedlar, A., Mundell, C. G. & Gallimore, J. F. 2001, *MNRAS*, 325, 151
- Beswick, R. J. 2006, *Proceedings of the 8th European VLBI Network Symposium September 26-29 (Torun: Poland)*, (eds.) Baan, W. et al., p.51
- Bryant, P. M., & Scoville, N. Z. 1999, *AJ*, 117, 2632
- Colbert, J. M. E., Wilson, A. S. & Bland-Hawthorn, J. 1994, *ApJ*, 436, 89
- Conway, J. E., Hurley, R., Parra, R., Diamond, P. J., Lonsdale, C. J., Lonsdale, C. J., *From Planets to Dark Energy: the Modern Radio Universe*. October 1-5 2007, The University of Manchester, UK. Published online at SISSA, *Proceedings of Science*, p.45
- Depoy, D. L., Becklin, E. E., Wynn-Williams, C. G. 1986, *ApJ*, 307, 116
- Fenech, D. M., Muxlow, T. W. B., Beswick, R. J., Pedlar, A. & M. K. Argo, M. K. 2008, *MNRAS*, 391, 1384
- Fried, J. W. & Schulz, H. 1983, *A&A*, 118, 166
- Gallimore, J. F. & Beswick, R. J. 2004, *AJ*, 127, 239
- Gallimore, J. F. Baum, S. A., & O'Dea, C. P. 2004, *ApJ*, 613, 794
- Gallimore, J. F., Axon, D. J., O'Dea, C. P., Baum, S. A. & Pedlar, A. 2006, *AJ*, 132, 546
- Greenhill, L. J., et al. 2003, *ApJ*, 590, 162
- Hagiwara, Y., Diamond, P. J., & Miyoshi, M. 2002, *A&A*, 383, 65
- Hagiwara, Y., Diamond, P. J., & Miyoshi, M. 2003, *A&A*, 400, 457
- Hagiwara, Y. 2007, *AJ*, 133, 1176
- Hagiwara, Y. 2010, *AJ*, 140, 1905
- Henkel, C., et al. 2005, *A&A*, 436, 75
- Ikebe, Y., et al. 2000, *MNRAS*, 316, 433
- Iono, D., et al. 2007, *ApJ*, 659, 283
- Kameno, S., Horiuchi, S., Shen, Z.-Q., Inoue, M., Kobayashi, H., Hirabayashi, H., & Murata, Y. 2000, *PASJ*, 52, 209
- Kellermann, K. I., & Pauliny-Toth, I. I. K. 1969, *ApJ*, 155, 71
- Komossa, S., Burwitz, V., Hasinger, G., Predehl, P., Kaastra, J. S. & Ikebe, Y. 2003, *ApJ*, 582, L15
- Kovalev, Y., Petrov, L., Gordon, D., & Fomalont, E. 2007, *VLBA Calibrator List* (Socorro: NRAO), <http://www.vlba.nrao.edu/astro/calib>
- Matt, G., et al. 2000, *MNRAS*, 318, 173
- Max, C. E., Canalizo, G., & de Vries, W. H. 2007, *Science*, 316, 1877

- McDonald, A. R., Muxlow, T. W. B., Pedlar, A., Garrett, M. A., Wills, K. A., Garrington, S. T., Diamond, P. J., Wilkinson, P. N. 2001, *MNRAS*, 322, 100
- Miyoshi, M. Moran, J., Herrnstein, J., Greenhill, L., Nakai, N., Diamond, P., Inoue, M. 1995, *Nature*, 373, 127
- Nakai, N., Sato, N., & Yamauchi, A. 2002, *PASJ*, 54, L27
- Nakanishi, K., Okumura, S. K., Kohno, K., Kawabe, R. & Nakagawa, T. 2005, *PASJ*, 57, 575
- Neff, S. G., Ulvestad, J. S., & Teng, S. H. 2004, *ApJ*, 611, 186
- Parra, R., et al. 2007, *ApJ*, 659, 314
- Pérez-Torres, M. A., Alberdi, A., et al. 2010, *A&A*, 519, L5
- Pradel, N., Charlot, P., & Lestrade, J.-F. 2006, *A&A*, 452, 1099
- Readhead, A. C. S. 1994, *ApJ*, 426, 51
- Sanders, D. B., Soifer, B. T., Elias, J. T., Madore, B. F., Mathews, K., Neugebauer, G. & Scoville, N. Z. 1988, *ApJ*, 470, 222
- Sanders, D. B., & Mirabel, I. F. 1996, *ARA&A*, 34, 749
- Scoville, N., et al. 2000, *AJ*, 119, 991
- Skinner, C. J., et al. 1997, *Nature*, 386, 472
- Smith, H. E., Lonsdale, C. J., Lonsdale, C. J., Diamond, P. J. 1998, *ApJ*, 493, L17
- Tacconi, L. J., Genzel, R., Tecza, M., Gallimore, J. F., Downes, D. & Scoville, N. Z. 1999, *ApJ*, 524, 732
- Tarchi, A., et al. 2010, *A&A*, 525, 91
- Thompson, A. R., Moran, J. M., & Swenson, G. W. 1986, *Interferometry and Synthesis in Radio Astronomy* (New York: Wiley Interscience)
- Ulvestad, J. S. 2009, *AJ*, 138, 1529
- Weiler, K. W., Panagia, N., Montes, M. J., & Sramek, R. A. 2002, *ARA&A*, 40, 387
- Yun, M. S., & Carilli, C. L. 2002, *ApJ*, 568, 88

Table 1: EVN Observations of NGC 6240

Epoch	Observing Date	Frequency (GHz)	Telescopes	Data rate (Mbit s ⁻¹)	Duration (hrs)	On-source (hrs)
1	30 Oct 2003	4.97	Ef,Hh,Mc,Nt,On,Wb	256	7.9	4.2
1	10 Nov 2003	1.64	Ef,Hh,Jb,Mc,Nt,On,Wb	256	8.2	3.6
2	16 Jun 2009	4.96	Ef,Jb,Mc,Nt,On,Sh,Tr,Ur,Wb	512	8.9	5.7
2	17 Jun 2009	2.24	Ef,Mc,Nt,On,Sh,Ur,Wb	512 ^a	8.7	5.8
2	17 Jun 2009	8.36	Ef,Mc,Nt,On,Sh,Ur	512 ^a	8.7	5.8

^aTotal recording rate at both S and X band.

Table 2: VLBI Imaging Parameters

Epoch	Frequency (GHz)	Rms (Uniform-weight) (mJy beam ⁻¹)	Beam size (FWHM) (mas)	PA (°)
1	1.6	0.13	30.8 × 17.8	50.9
1	5.0	0.083	10.5 × 4.58	50.1
2	2.2	0.55	10.97 × 7.48	70.1
2	5.0	0.055	6.11 × 4.93	72.1
2	8.4	0.11	3.42 × 2.77	70.0

^aThe rms noise levels near the reference position used in the JIVE VLBI correlation.

Table 3: Positions of VLBI Components in NGC 6240

Component	Coordinate		Accuracy	
	α (J2000)	δ (J2000)	$\Delta\alpha\cos\delta^\dagger$	$\Delta\delta^\dagger$
Frequency	16 ^h 52 ^m	02°24'	(mas)	(mas)
Northern nucleus (N2)				
1.6 GHz	58.9242	04.779	0.9	0.7
2.2 GHz	58.9240	04.777	1.2	0.9
5.0 GHz (Oct 2003)	58.9240	04.776	0.6	0.6
5.0 GHz (Jun 2009)	58.9240	04.776	0.6	0.6
8.4 GHz	58.9240	04.776	0.6	0.6
Southern nucleus (N1)				
1.6 GHz	58.8903	03.351	1.1	1.1
5.0 GHz (Oct 2003)	58.8901	03.348	0.7	0.6
5.0 GHz (Jun 2009)	58.8902	03.350	0.6	0.6
Radio source 1 (RS1)				
5.0 GHz (Oct 2003)	58.8886	03.326	0.7	0.6
5.0 GHz (Jun 2009)	58.8885	03.326	0.6	0.6
8.4 GHz	58.8885	03.327	0.6	0.6
Radio source 2 (RS2)				
1.6 GHz	58.8991	03.607	2.0	1.3
5.0 GHz (Oct 2003)	58.8993	03.602	0.8	1.3
5.0 GHz (Jun 2009)	58.8994	03.602	0.6	0.6

[†]The position error in right ascension ($\Delta\alpha\cos\delta$) and declination ($\Delta\delta$).

TABLE 4
COMPONENT FLUX DENSITIES OF NGC 6240

Epoch 1 (EVN; Oct–Nov 2003)				Epoch 2 (EVN; June 2009)				MERLIN
Name (1)	$S_{1.6}$ (2)	$S_{5.0}$ (3)	$\alpha_{5.0}^{1.6}$ (4)	$S_{2.2}$ (5)	$S_{5.0}$ (6)	$S_{8.4}$ (7)	$\alpha_{8.4}^{5.0}$ (8)	$S_{5.0}$ (9)
N1	2.09	2.63	0.20	< 2.75	2.85	< 0.55	< -3.2	36.8
N2	3.95	5.99	0.37	4.59	5.79	1.78	-2.3	16.1
RS1	...	2.34	...	< 2.75	3.00	3.57	0.34	...
RS2	1.07	0.38	-0.91	< 2.75	0.59	< 0.55	< -0.14	...

VLBA							
Epoch 1 (Aug 1999)		Epoch 2 (Apr–May 2000)		Epoch 3 (Dec 2000–Jan 2001)			
(10)	$S_{1.7}$ (11)	$S_{2.4}$ (12)	$S_{1.7}$ (13)	$S_{2.4}$ (14)	$S_{1.7}$ (15)	$S_{2.4}$ (16)	
S1	...	0.63±0.13	0.62±0.06	0.59±0.10	0.40±0.08	0.47±0.08	
RS3	0.46	
RS4	0.44	0.29	

NOTE.—Flux densities are in mJy. Col. (1): Source names from Baan, Hagiwara, & Hofner (2007) for N1 (southern nucleus) and N2 (northern nucleus). RS1 and RS2 are newly detected sources in these EVN observations. Flux density errors measured by the EVN are estimated at $\sim 10\%$. Col. (2),(3): The 1.6 GHz and 5.0 GHz flux densities at Epoch 1 as measured by the EVN. Col. (5)-(7): The 2.2 GHz, 5.0 GHz, and 8.4 GHz flux densities at Epoch 2 as measured by the EVN. Col. (4),(8): The spectral indices between 1.6 GHz and 5.0 GHz (Epoch 1) and between 5.0 GHz and 8.4 GHz (Epoch 2). Col. (9): Data taken from MERLIN observations at 5.0 GHz in Beswick et al. (2001). All flux density upper limits are 5σ . Col. (10): Data taken from VLBA observations in Gallimore & Beswick (2004). RS3 ($\approx 0''.02$ northwest of the southern nucleus N1) and RS4 ($\approx 0''.03$ northwest of the northern nucleus N2) are newly defined in this article. Col. (11)-(16): The 1.7 GHz and 2.4 GHz flux densities as measured by the VLBA (Gallimore & Beswick 2004).

TABLE 5
SOURCE SIZES OF N1, N2, RS1, AND RS2

	N1			N2			RS1			RS2		
(1) Frequency (Epoch)	(2) (mas ²)	(3) (pc ²)	(4) (°)	(5) (mas ²)	(6) (pc ²)	(7) (°)	(8) (mas ²)	(9) (pc ²)	(10) (°)	(11) (mas ²)	(12) (pc ²)	(13) (°)
1.6 GHz (Oct 2003)	17.6×12.6	8.4×6.0	43	39.3×13.5	18.7×6.4	5	—	—	—	15.8×7.0	7.5×3.3	169
5.0 GHz (Oct 2003)	9.2×5.9	4.4×2.8	137	19.5×6.6	9.3×3.2	98	9.2×3.9	4.4×1.9	80	9.2×6.1	4.4×2.9	140
5.0 GHz (Jun 2009)	7.6×5.2	3.6×2.5	161	12.4×3.4	5.9×1.6	101	3.6×1.9	1.7×0.9	70	2.5×2.9	1.2×1.4	128
8.4 GHz (Jun 2009)	—	—	—	6.6×1.4	3.1×0.7	85	3.2×1.3	1.5×0.6	58	—	—	—

NOTE.—Source sizes are upper limit values and they are deconvolved using the VLBI synthesized CLEAN beam. Col. (1): The observing frequency and Epoch. Col. (2),(5),(8),(11): Major axis × minor axis values, in milli-arcsecond (mas). Col. (3),(6),(9),(12): Major axis × minor axis values, in parsecs (pc). Col. (4),(7),(10),(13): The position angles of the sources.

Table 6: Properties of the VLBI sources N1, N2, RS1, and RS2

Source	$T_{b,5\text{GHz}}$ ($\times 10^6$ K)	P (5.0 GHz) ($\times 10^{21}$ W Hz $^{-1}$)	$T_{b,8.4\text{GHz}}$ ($\times 10^6$ K)	P (8.4 GHz) ($\times 10^{21}$ W Hz $^{-1}$)
Northern nucleus (N2)	10.0	2.9	4.9	1.7
Southern nucleus (N1)	5.2	1.7	<1.5	<0.70 [†]
Radio source 1 (RS1)	31.6	3.9	21.8	4.1
Radio source 2 (RS2)	5.9	0.75	<1.5	<0.70 [†]

NOTE.—These values are calculated from data obtained in June 2009. [†]5 σ upper limit

TABLE 7

MODELING FIT PARAMETERS FOR THE NUCLEI N1 AND N2

Parameter	Value	
Free-free absorption model	N1	N2
S_0	25.4 ± 35.7 mJy	30.4 ± 60.8 mJy
α	-1.4 ± 0.8	-1.1 ± -1.1
τ_{ff}	5.3 ± 3.5	4.5 ± 4.9
Reduced χ^2	0.59	3.8
Synchrotron self-absorption model	N1	N2
S_0	0.39 ± 0.07 mJy	0.74 ± 0.22 mJy
α_0	-3.2 ± 2.3	-2.40 ± 1.97
τ_s	1349 ± 5110	400 ± 1326
Reduced χ^2	0.43	2.9

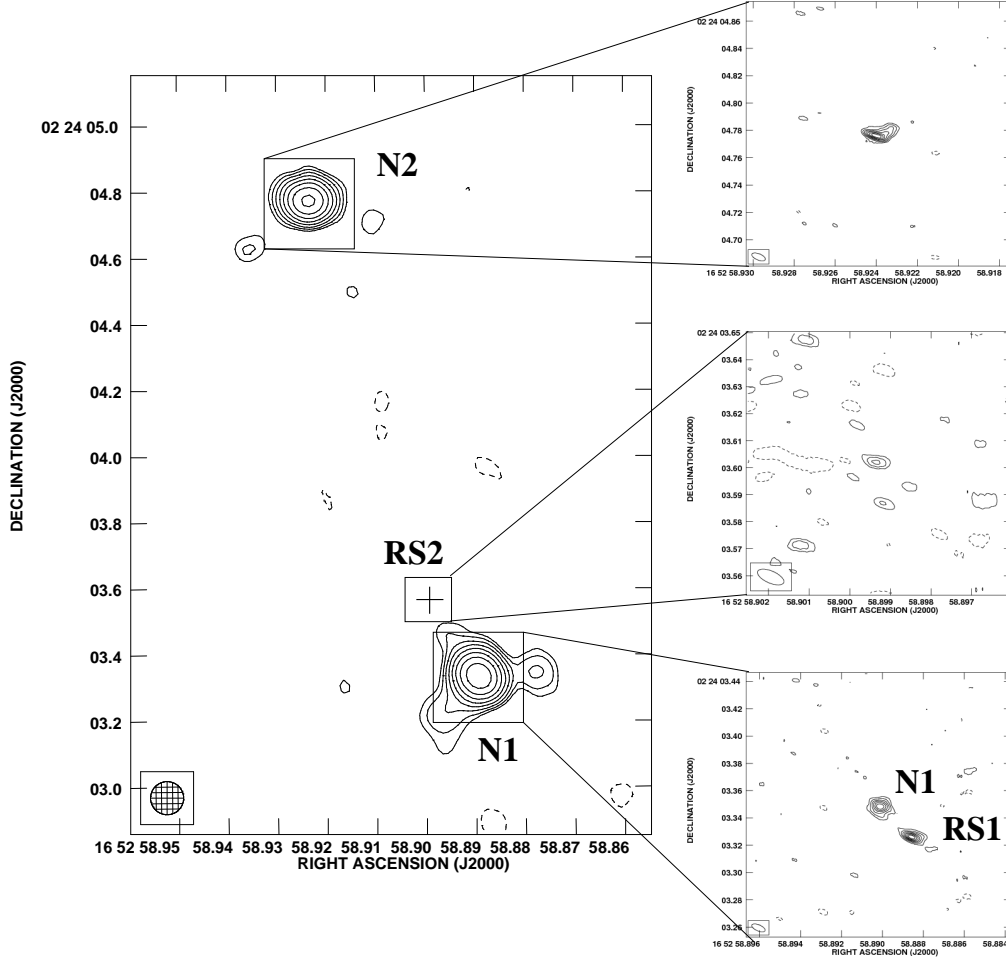


Fig. 1.— The radio structure of the nuclear region of NGC 6240 at 5 GHz as obtained by MERLIN (Gallimore & Beswick 2004) with the location of compact components detected by the new 5 GHz EVN observations in October 2003 (Epoch 1) as presented in the right-hand-side frames. The synthesized beam (FWHM) of the observations is plotted in the left bottom corner of all maps. The two radio nuclei N1 (southwest) and N2 (northeast) have been labelled following the designation of Colbert et al. (1994) and Baan et al. (2007). Note that in Gallimore & Beswick (2004) the northern nucleus is labeled as N1 and the southern nucleus labeled as S. The cross indicates the positions of radio source RS2 that appeared in our observation. The contours in the MERLIN image are at $0.5 \text{ mJy beam}^{-1} \times -1, 1, 2, 4, \dots, 32$. The contours of the three VLBI components are given with Figures 2, 3, and 4.

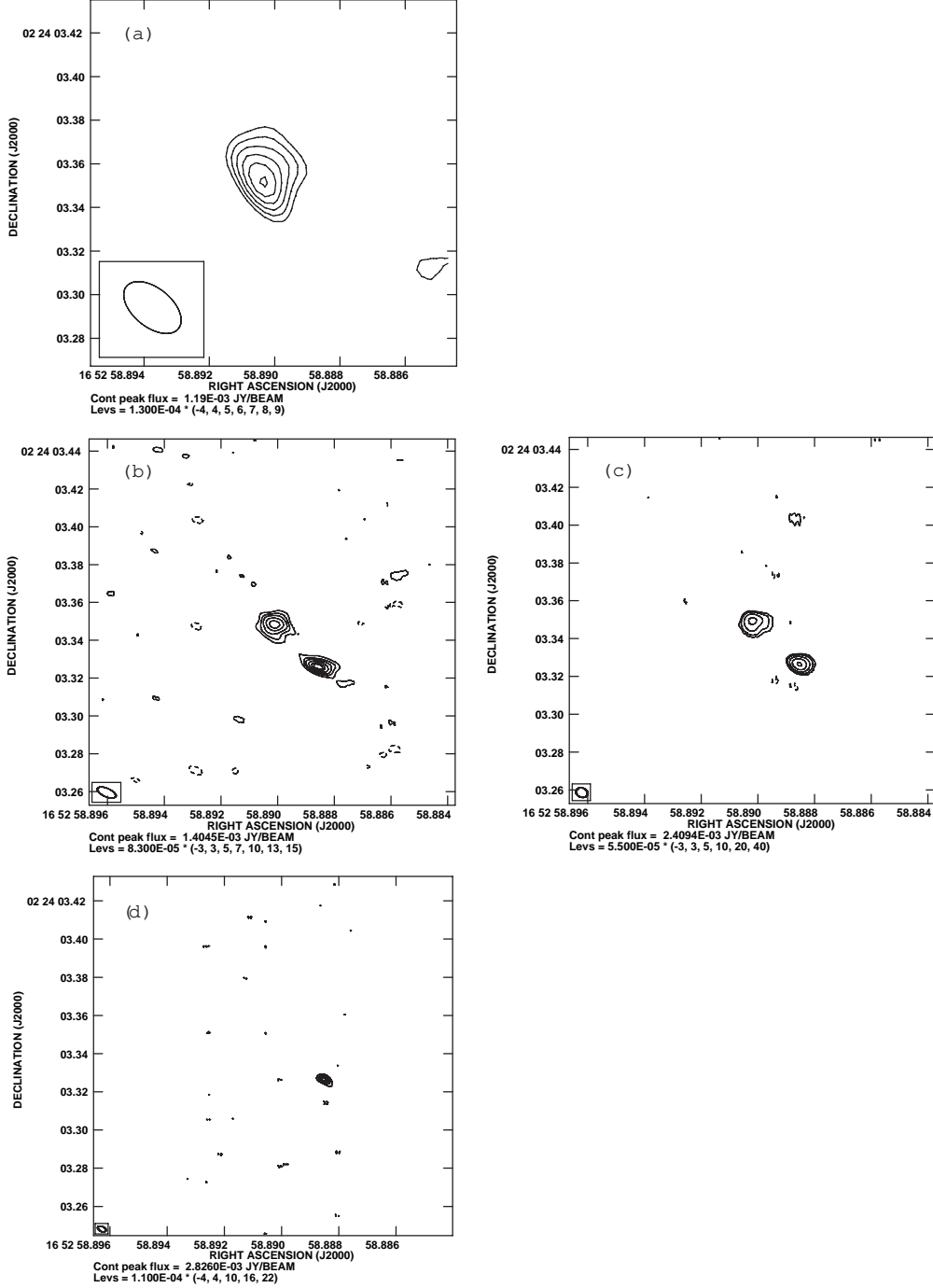


Fig. 2.— Radio continuum images of the southwestern nucleus N1 of NGC 6240 and the compact radio source RS1, which is located southwest of N1. The synthesized beams are plotted at the bottom-left corner on each panel. (a) The 1.6 GHz image of N1 observed in Epoch 1 in 2003. (b) The 5.0 GHz images of N1 and RS1 observed in Epoch 1 in 2003. (c) The 5.0 GHz images of N1 and RS1 observed in Epoch 2 in 2009. (d) The 8.4 GHz image of RS1 obtained in Epoch 2.

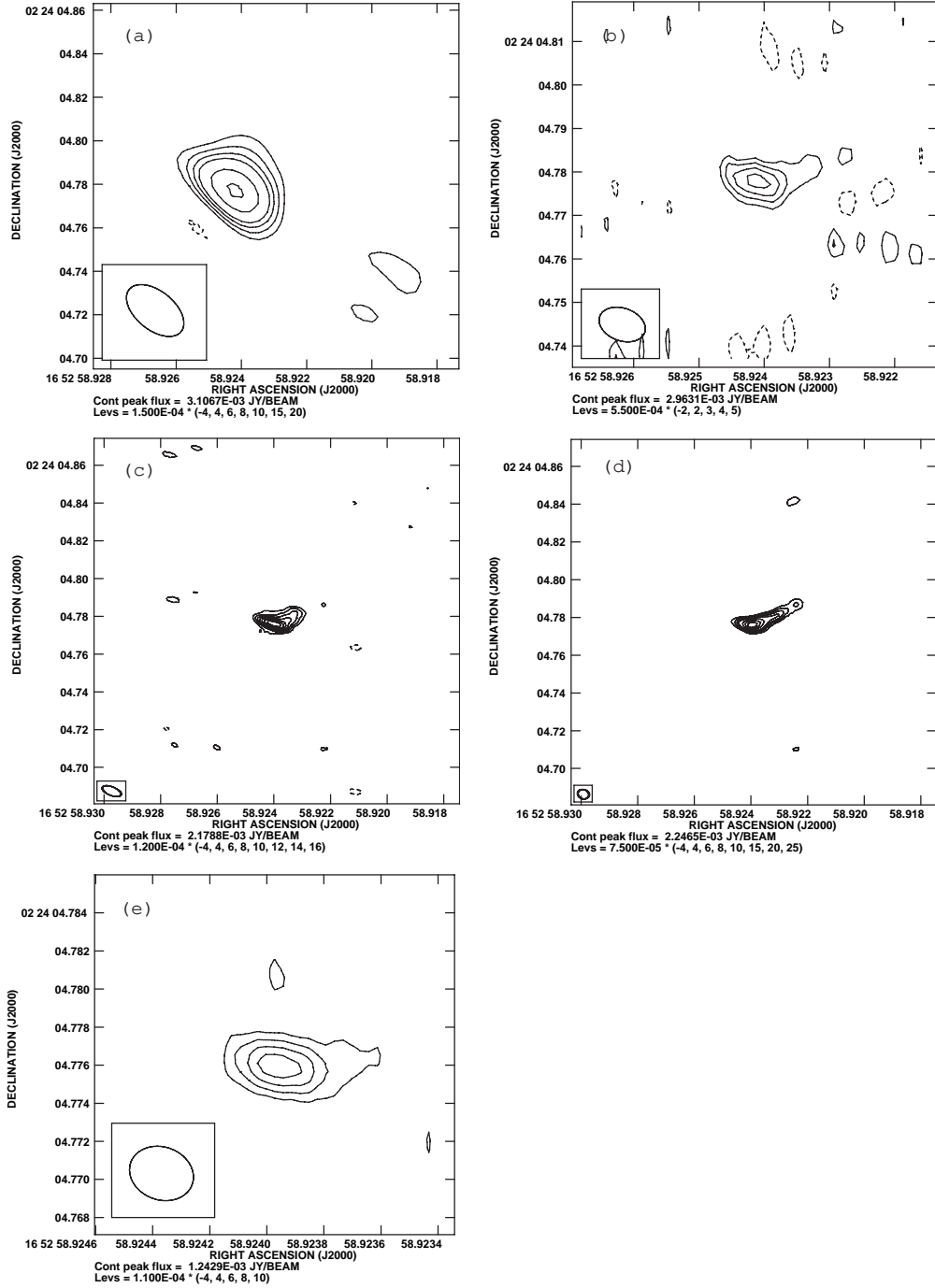


Fig. 3.— Radio continuum images of the northeastern nucleus N2 of NGC 6240. The synthesized beams are plotted at the bottom-left corner on each panel. (a) The 1.6 GHz image observed in Epoch 1 in 2003. (b) The 2.2 GHz image observed in Epoch 2 in 2009. (c) The 5.0 GHz image observed in Epoch 1 in 2003. (d) The 5.0 GHz image observed in Epoch 2 in 2009. (e) The 8.4 GHz image obtained in Epoch 2 in 2009.

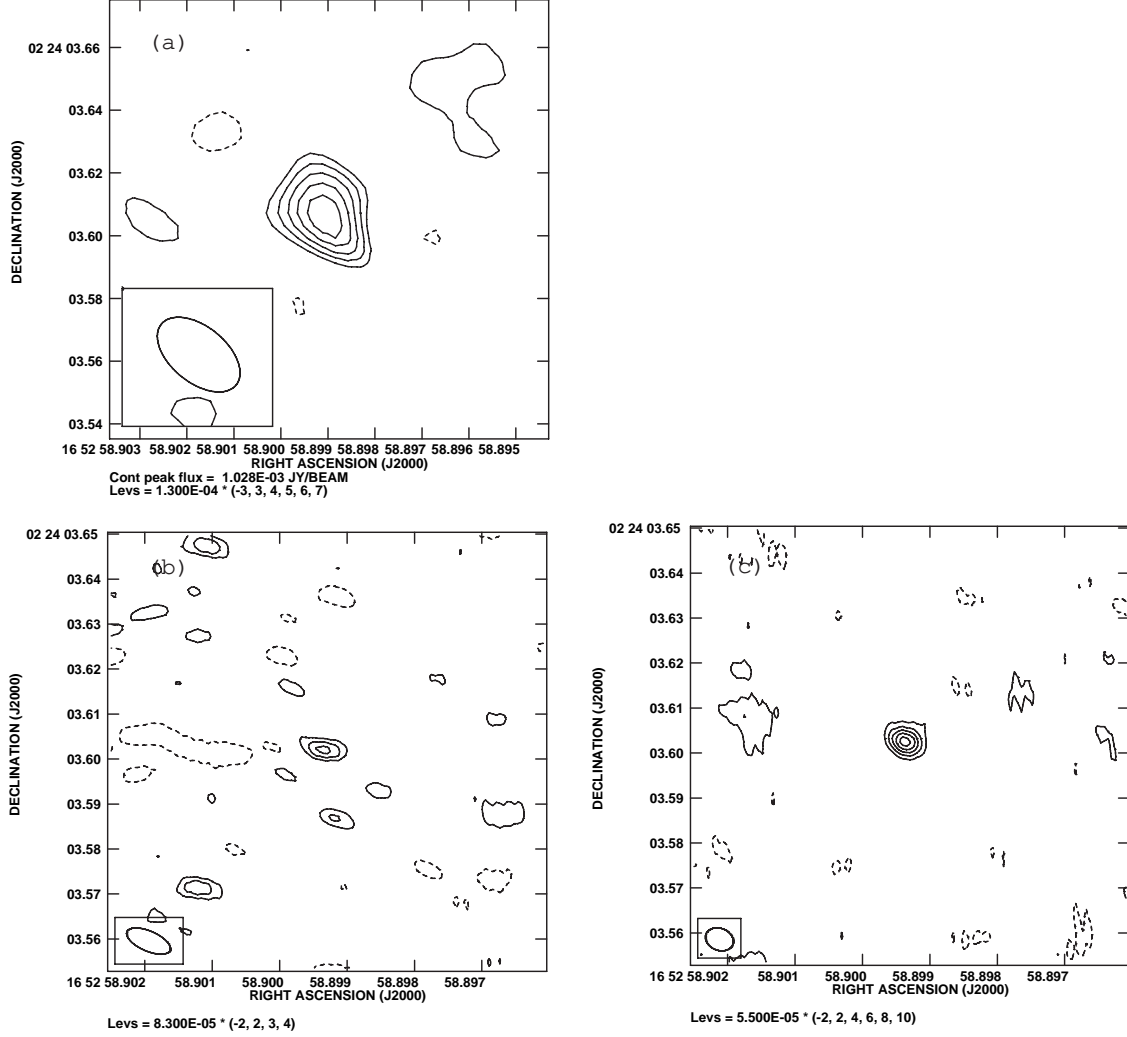


Fig. 4.— Radio continuum images of the radio source RS2 that is located northeast of the southern nucleus N1 as indicated in the lower angular resolution map obtained by the 5 GHz MERLIN (Figure 1). The synthesized beams are plotted at the bottom-left corner on each panel. (a) The 1.6 GHz image obtained in Epoch 1 in 2003. (b) The 5.0 GHz image of Epoch 1 in 2003. (c) The 5.0 GHz image of Epoch 2 in 2009.

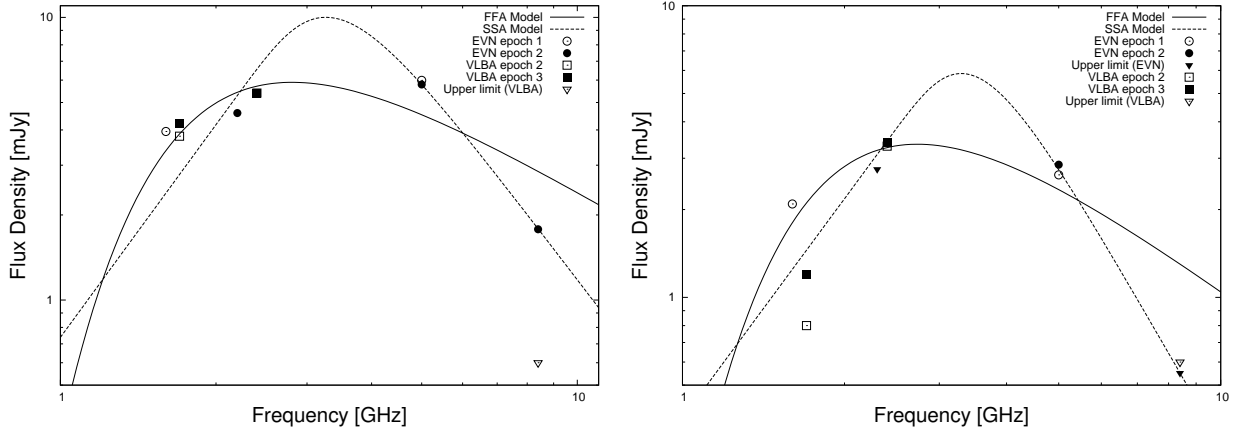


Fig. 5.— Radio spectra of the two nuclei of NGC 6240.

Left frame: The spectrum of the northern nucleus N2. The solid lines represent the free-free absorption (FFA) model as fitted to the Epoch 2 data and 1.6 GHz data in Epoch 1, assuming no significant flux density variation of N2 between the two observing epochs. The dotted line represents the synchrotron self-absorption (SSA) model as fitted to the same data as the case of FFA.

Right frame: The spectrum of the southern nucleus N1. The solid and dotted lines represent the FFA model and SSA model as fitted to data of the two EVN epochs including upper limit values, assuming no significant flux density variation of N1 during these two epochs.

The data points: The filled circles at 2.2, 5.0, and 8.4 GHz are data points from the EVN during Epoch 2 (2009). The open circles at 1.6 and 5.0 GHz are data points from the EVN during Epoch 1 (2003). The open squares at 1.7 and 2.4 GHz are the data points from the VLBA at Epoch 2 (April to May 2000), and filled squares at 1.6 and 2.4 GHz are from the VLBA data of Epoch 3 (December 2000 to January 2001). The triangles denote the 5σ upper limit values obtained at 2.2 and 8.4 GHz with the VLBA in August 1999 from Gallimore & Beswick (2004).

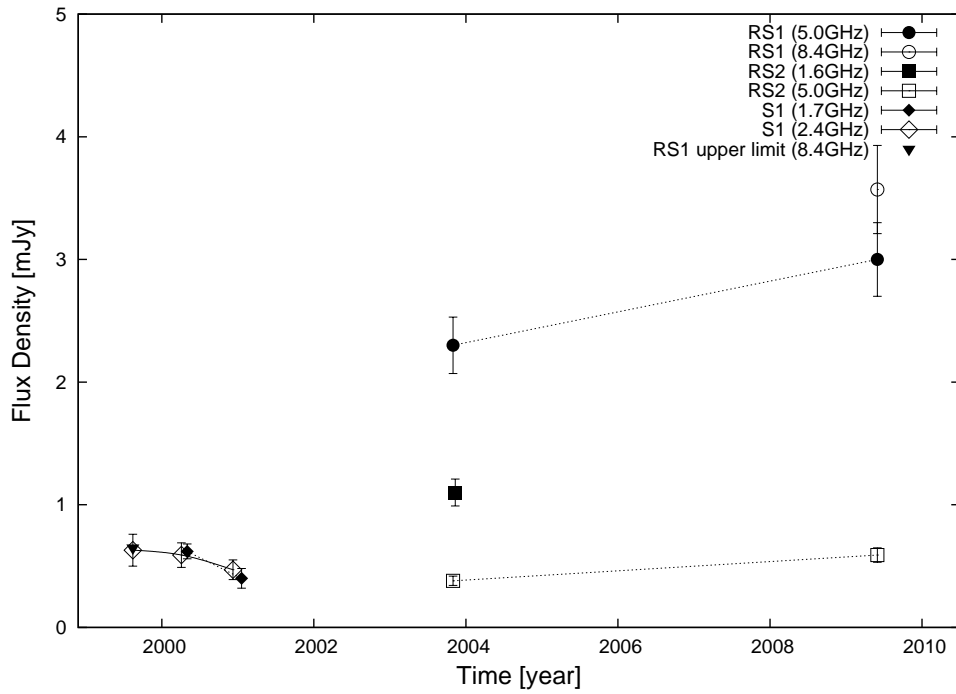


Fig. 6.— Radio light curves of RS1, RS2, and S1. Filled circles denote the 5.0 GHz flux density of RS1, and an open circle denotes the 8.4 GHz flux density of RS1. A filled square shows the 1.6 GHz flux of RS2, and the open squares denote the 5.0 GHz flux of RS2. Filled and open diamonds denote the 1.7 GHz and 2.4 GHz flux of S1 from the earlier VLBA data. A open triangle indicates the upper limit (5σ) of the 8.4 GHz earlier VLBA data.